Journal of Cleaner Production 295 (2021) 126409

Contents lists available at ScienceDirect

Journal of Cleaner Production

journal homepage: www.elsevier.com/locate/jclepro

Empirical data-driven multi-layer perceptron and radial basis function techniques in predicting the performance of nanofluid-based modified tubular solar collectors

Gholamabbas Sadeghi [a, *], Anna Laura Pisello [b], Saeed Nazari [c], Mohammad Jowzi [d], Farzin Shama [e]

[a] Department of Thermal and Fluid Engineering, Faculty of Engineering Technology, University of Twente, P.O. Box 217, 7500, AE Enschede, the Netherlands
[b] Department of Engineering, University of Perugia, Via g. duranti 91-06125, Perugia, Italy
[c] Department of Mechanical Engineering, Faculty of Engineering, University of Kurdistan, Sanandaj, Iran
[d] Department of Mechanical Engineering, Faculty of Engineering, Razi University, Kermanshah, Iran
[e] Department of Electrical Engineering, Kermanshah Branch, Islamic Azad University, Kermanshah, Iran

ARTICLE INFO

Article history:
Received 6 April 2020
Received in revised form
2 February 2021
Accepted 14 February 2021
Available online 18 February 2021

Handling editor. Dr Sandra Caeiro

Keywords:
Solar water heater
Modified evacuated tube solar collector (METSC)
Cu_2O/DW nanofluid
MLP and RBF algorithms
Performance parameters optimization

ABSTRACT

In the present study, the modified evacuated tube solar collector (METSC) with a bypass pipe utilizing copper oxide/distilled water (Cu_2O/DW) nanofluid is experimented. Then, the performance of METSC was predicted through Artificial Neural Networks (ANNs) techniques. The input variables were different volumes of the storage tank from 5 to 8 l, various diameters of the bypass pipe from 6 to 10 mm, and various volumetric concentration of the nanofluid from 0 to 0.04. Also, the output variables were the temperature difference of fluid in 1-h period and the energetic efficiency of METSC. The results demonstrated that the METSC performance was mostly impacted by the tank volume alteration. Moreover, the optimum bypass tube diameter value was obtained, and it was denoted that using the Cu_2O/DW nanofluid enhances the daily energy efficiency of METSC up to 4%. Furthermore, it was shown that both MLP and RBF techniques are two reliable algorithms to predict the thermal characteristics of an METSC. The maximum amounts of mean relative percentage error for MLP and RBF algorithms were reported as 0.576 and 0.907, respectively. Hence, two mathematical models were reported for formulating the output variables in terms of the input variables using the MLP technique.

1. Introduction

With the fast progress of near zero energy buildings implementations (Hamburg et al., 2020; Lidberg et al., 2019), the energy need associated to space heating and cooling is progressively decreasing (López-Ochoa et al., 2019; Ma et al., 2020), thanks to both passive and active solutions (Rosso et al., 2014) and renewables integration (Cabeza et al., 2018; Sadeghi and Nazari, 2021). Therefore, hot water production requires an important energy demand factor in mild climates and in high performance new constructions and retrofits (Pigliautile et al., 2019).

Heating water needs energy; hence, finding novel approaches in harvesting energy, is very important for water heaters. From a conventional point of view, electrical energy, or fossil fuel energy ought to be used for operating water heaters. However, renewable energy is a good and clean source of alternative energy (Johnsson and Adl-Zarrabi, 2020), which can be exploited in areas exposed to a lot of sunlight, such as Iran, Iraq, Texas, Melbourne and other tropical areas. Evacuated tube solar collectors (ETSCs) are nowadays very popular in solar energy-driven world for supplying household hot water (Sabiha et al., 2015; Sadeghi et al., 2020d).

Many studies have been conducted upon enhancement of the thermal performance of the ETSCs, such as using nanofluids, using different types of concentrators, utilizing phase change materials, structural improvement of the system, etc. (Kabeel et al., 2020; Olfian et al., 2020). Nanofluids are basically used to enhance the thermal characteristics of heat transfer fluid (Nazari et al., 2019a; Qiu et al., 2020) in order to retrofit different mechanical-thermal systems (Ghafurian et al., 2020; Sheikholeslami and Mahian, 2019). One of the major factors leading to deterioration of the

* Corresponding author.
E-mail address: g.sadeghi@utwente.nl (G. Sadeghi).

https://doi.org/10.1016/j.jclepro.2021.126409

Nomenclature

Symbols

$\mathbf{A_c}$	The collector area (m^2)
b	
$\mathbf{C_p}$	Specific heat (J kg^{-1} K^{-1})
$\mathbf{C_{p,np}}$	Specific heat of nanoparticle (J kg^{-1} K^{-1})
$C_{p,nf}$	Specific heat of nanofluid (J kg^{-1} K^{-1})
$C_{p,bf}$	Specific heat of base fluid (J kg^{-1} K^{-1})
C_j	Center vector for the jth hidden node
D	Bypass tube diameter (m)
F_R	Removal factor
F_n	Activation functions of hidden layers
G	Solar radiation intensity (W m^{-2})
I	Unit matrix
I-C_j	Euclidean norm
M_T	Mass of the fluid inside the tank (kg)
n	Number of hidden layers
N	Experiments number
Q_n	Collector heat gain (J)
T_a	The ambient temperature (° C)
T_i	Initial temperature of the fluid (° C)
T_j	Final temperature of the fluid (° C)
$T_{i,j}$	Temperature of the working fluid (° C)
t	Time (second)
ΔT	Fluid temperature difference in 1 h (° C)
u	Uncertainty amount
U_l	Overall heat loss coefficient
V	Volume of the thermal storage tank (m^3)
W_i	Weighting factors
X_i(Ex)	Experimental data
X_i(pr)	Predicted data
Y_i	The ith output

Subscripts

ef	Effective
j	Number of inputs
K	Number of outputs

Acronyms

ANN	Artificial Neural Network
AI	Artificial intelligence
Cu_2O	Copper oxide nanoparticles
DW	Distilled water
ETSC	Evacuated tube solar collector
Eff	Energy efficiency
Ex	Experimental
GP	Genetic programming
GA	Genetic algorithm
HP	Heat pipe
METSC	Modified evacuated tube solar collector
LM	Levenberg-Marquardt
l	Liter
MA	Measurement accuracy of each device
MARS	Multi-variate adaptive regression spline
MLP	Multi-layer Perceptron
MRPE	Mean relative percentage error
MAPE	Mean absolute percentage error
MT	Model tree
PSO	Particle swarm optimization
Pr	Predicted
RBF	Radial basis function
RMSE	Root mean square error
Temp	Maximum fluid temperature difference

Greek letters

α	Thermal diffusivity (m^2 s^{-1})
η	Thermal Energy efficiency
ρ_{bf}	Base fluid density (kg m^{-3})
ρ_{nf}	Nanofluid density (kg m^{-3})
ρ_{np}	Nanoparticles density (kg m^{-3})
σ^2	Variance of Gaussian function
τ	Transmittance coefficient
ϕ	Volume concentration of nanofluid

performance of ETSC is the stagnation point at the end of tubes (Morrison et al., 2004). One study surveyed the impact of removing this point at the lower area of the evacuated tube. It was found that this approach to modifying the ETSC makes the fluid temperature distribution inside the tank and the evacuated tubes more uniform (Sato et al., 2012). Jowzi et al. (2019) experimentally removed the stagnant point at the lower area of the evacuated tube in an one-tube ETSC by use of a bypass tube, which connected the tank to the end of the tube. The results demonstrated that this approach can raise the energy efficiency of ETSCs up to 11%. S. Iranmanesh et al. (2017) could experimentally enhance the conductivity of the graphene nanoplatelets up to 27%, and reached the 90% energy efficiency of the ETSC using this type of nanofluid at 0.1% weight fraction of the nanoparticles. Sharafeldin and Grof (2018) utilized Cesium oxide/water nanofluid to augment the performance of an ETSC. They showed that the thermos-physical characteristics of the ETSC increase about 34% by use of the proposed nanofluid at volume concentration of 0.035%. Many surveys have proven the copper-based nanofluids effectiveness in presenting a more system performance due to the high thermal conductivity of copper (Nazari et al., 2019b). Sadeghi et al. (2019a) enhanced the thermodynamical performance of an ETSC utilizing Cu_2O/distilled water nanofluid 11%. Furthermore, the effect of various volume fractions of this nanofluid on its thermo-physical characteristics was examined. Eidan et al. (2018) used two types of nanofluids, namely Al_2O_3/aceton-based and CuO/aceton-based in a heat pipe evacuated tube solar collector (HP-ETSC). The findings indicated that using the first nanofluid is more beneficial to the solar system, and as to the latter one, the problem of sedimentation of nanoparticles deteriorates at 2% volume fraction of nanofluid.

Inasmuch as experimentally collecting much data and their analyzing for achieving the optimum performance parameters of a system might be a little time consuming, some artificial intelligence (AI) techniques, such as ANNs, gene-expression programming (GEP), genetic algorithm (GA), particle swarm optimization (PSO), model tree (MT), multi-variate adaptive regression spline (MARS), etc. can model and predict the performance of the system in a very lower period of time. On the basis of a review research on the application of ANN techniques, it was shown that these techniques are capable of forecasting the performances of the solar systems, such as solar water heaters, and solar air heaters (Ghritlahre and Prasad, 2018a; Ghritlahre et al., 2018b). It is also indicated that ANN and AI are very fast tools to model, simulate, and optimize the performance parameters of the solar systems in comparison to the conventional approaches (Nazari et al., 2020; Sadeghi et al., 2020b). The major duty of ANN is to train the structure gathered by either

experimental, or numerical data (Ghritlahre et al., 2018c). Abdollahi-Moghaddam et al. (2018) surveyed the convective heat transfer of CuO/water nanofluid used in a horizontal tube. The results demonstrated that using the proposed nanofluid can ameliorate the heat transfer up to 2.8 times more than that for water. They also developed an ANN model to forecast the Nusselt number, and the model indicated the maximum deviation of 1%. Heng et al. (2019) proposed an ANN method to foreseen the daily outlet water temperature of a parabolic trough collector in 1 min. The amount of absolute deviation for the ANN model was less than 2 K. The input parameters were the velocity of the fluid, and the inlet water temperature. Moreover, the annual outlet temperature of the fluid can be predicted in 6 h by the propose model. Sadeghi et al. (2020c) experimentally showed that both MLP and RBF techniques can reasonably predict the performance parameters of an ETSC. However, they indicated that the MLP technique more accurately predicts the ETSC efficiency compared to the RBF one. Moreover, Sadeghi et al. (2020a) examined the capability of GEP, MT, and MARS techniques in forecasting the inlet outlet temperature difference and the energy efficiency of ETSC using the experimental data. They proposed mathematical equations for each output in terms of volume of the tank, mass flow rate, and volume fraction of nanoparticles. The amounts of root mean square errors for prediction of the energy efficiency equations based on MT, GEP, and MARS techniques were reported as 0.029, 0.035, and 0.018.

In this study, the Cu_2O/DW nanofluid was used as the working fluid inside an METSC using a bypass tube to eliminate the stagnant region formed on the bottom of the tube. The main novelties are obtaining the optimum bypass tube diameter to present the highest efficiency and formulating the performance parameters of similar METSCs through well-known reliable approaches. In other words, one of the main goals of this project was to figure out whether the performance parameters (the temperature difference of the fluid inside the storage tank over the interval of 1 h, and the energy efficiency) of an METSC can be predicted and modelled through the MLP and RBF techniques in terms of different input parameters, namely volume of the thermal storage tank, diameter of the bypass tube, and different volume concentrations of the Cu_2O/DW nanofluid.

2. Nanofluid synthesis and stability procedures

Nanofluids tend to enhance the performances of solar thermal systems through modifying the thermal properties of the working fluid in a thermally improved direction. However, their preparation and synthesis procedure are of enormous importance to ensure their stability. Otherwise, using them in the solar systems might backfire. In the present work, copper-based nanofluid was selected due to highly effective conductivity of copper compared to other types of metals (Zhao et al., 2019). Furthermore, a two-step approach was utilized to synthesize a stabilized Cu_2O/DW nanofluid due to presenting more efficient outcome compared with the one-step method (SANJEEVI and LOGANATHAN, 2020). As for preparation, one type of surfactant (polyvinylpyrrolidon) was added to double-aqueous copper solution. Fig. 1 (a) indicates the monohydrate copper (II) crystals used in this work, which was manufactured by Milipore Company. The synthesized surfactant-copper solution was stirred with a magnetic stirrer. Next, an ammonia solution with 37% concentration was added to the solution, and the whole material was placed under ultrasonic waves with 60 kHz frequency for half an hour. In the next step, ascorbic acid with the chemical formulation of $C_6H_8O_6$ was added, and the prepared nanofluid was again dealt with ultrasonic waves for around 15 min.

The high sediment of nanoparticles inside the primary fluid testifies less improving the thermal characteristics of nanofluid; hence, less productivity of the solar system. On the other hand, it is very important to apply the prepared nanofluid to the system right after preparation because it will be at the maximum efficiency at that time, and it will gradually starts to settle on the bottom implying ineffectiveness of the nanofluid. Fig. 1 (b) and (c) illustrate the proposed nanofluid 29 min after preparation, and six months after preparation, respectively proving the stability of the utilized nanofluid over a long period of time through observation.

Moreover, X-Ray Diffraction (XRD), Fourier Transform Infrared (FT-IR), and Transmission Electron Microscope (TEM) investigations have been adopted to ensure the accurately correct synthesis of the prepared nanofluid. The XRD analysis ought to be conducted in order to determine the phase, structure, size, single oriented, and constant of crystals. For this aim, 1 gr of dried Cu_2O nanoparticles were analyzed through an XRD device (Inlet Model) with 1.54 A wavelength. As demonstrated in Fig. 2, the acquired spectrum agrees to the standardized Cu_2O peaks in the literature (Shah and Al-Ghamdi, 2011). Furthermore, the functional groups were detected through the FT-IR analysis within wavelengths 500 to 4000 cm^{-1}. As shown in Fig. 3, the wavelength of 620 cm^{-1} is assigned to the Cu_2O characteristic peak (Khan et al., 2015). In addition, the peaks regarding the polyvinylpyrrolidon are indicated on 1293, 1442, 1661, and 2921 cm^{-1} wavenumbers as well as the 3435 cm^{-1} wavelength is pertaining to the OH groups (the functional groups). Ultimately, the TEM test of the Cu_2O nanoparticles was undertaken to investigate the morphology of the nanoparticles. Overview of 30 nm, it was indicated that the spherical nanoparticles possess dimensions of less than 50 nm (see Fig. 4).

3. Experimental setup

Fig. 5 illustrates the scheme of a single tube METSC, which is generically comprised of one modified tube (open end) made of glass, an insulated storage tank made of polyethylene, a bypass tube made of polyethylene, and a frame made of iron. The bypass tube was used for connection of the tank to the lower area of the tube without disrupting the vacuum existing between the cover and the absorber. The METSC was constructed for various amounts of volumes of tanks, diameters of the bypass tubes, and fractions of the nanoparticles. The setup was placed on a frame with 45° tilt angle (see Fig. 2). The experimentations were undertaken during June, July, and August in 2018 and 2019 under clear sky in Kermanshah city with 34.2 ^{o}E latitude and 47.1 ^{o}N longitude. The main properties of the constructed METSC are illustrated in Table 1.

Furthermore, the volumes of the storage tanks were considered as 5, 6, 7, and 8 l; the diameters of the bypass tubes were regarded as 6, 7, 8, 9, and 10 mm; and the volume concentrations of the nanofluid were considered as 0, 0.01, 0.02, 0.03, and 0.04 for the experiments. The insulation of the storage tanks was conducted through polyethylene cover with 1 cm thickness. Seven K-type thermocouples, the measurement accuracy of which were 0.1 °C, were utilized for measuring the temperature of the working fluid inside the solar collector and the ambient temperature. There existed three thermocouples inside the evacuated tube, and three thermocouples inside the thermal storage tank. It ought to be mentioned that the tank was not stratified and the bulk temperature of the fluid inside the tank was the sole preference to measure. The other thermocouple was used to record the ambient temperature during the experimentations. As indicated in Fig. 6 (a), the data logger model BTM-4208SD produced by Lutron Corporation was employed to record the temperatures, and the solar radiation was measured every 5 min over the day of experiments from 9:00 to 18:00 by the TES 1333R pyranometer. The mean temperature of fluid inside the storage tank was acquired in accordance with

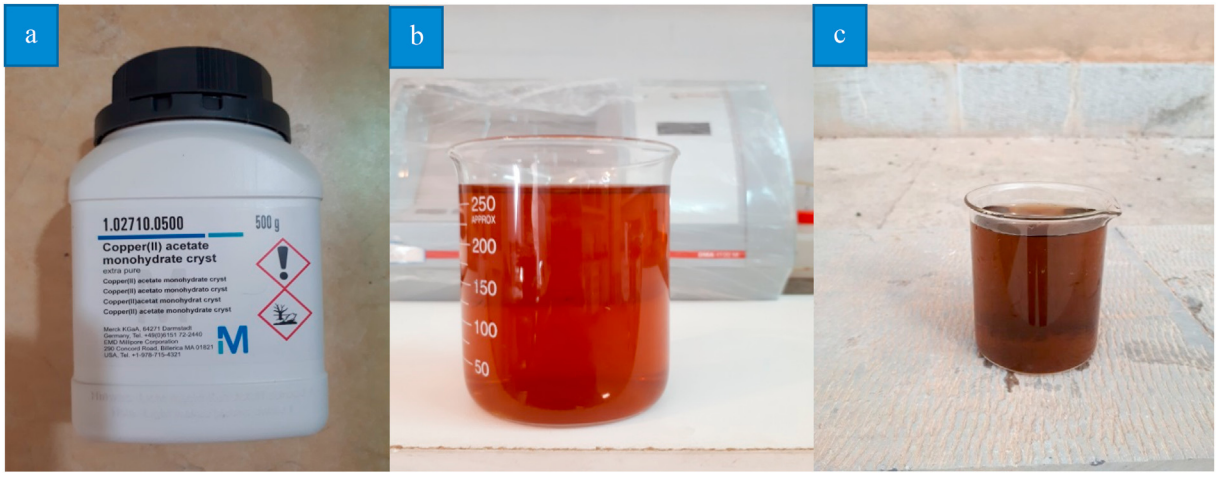

Fig. 1. (a) Double-aqueous copper crystal, (b) Image of Cu_2O/DDW 30 min after preparation, (c) Image of Cu_2O/DDW 6 months after preparation.

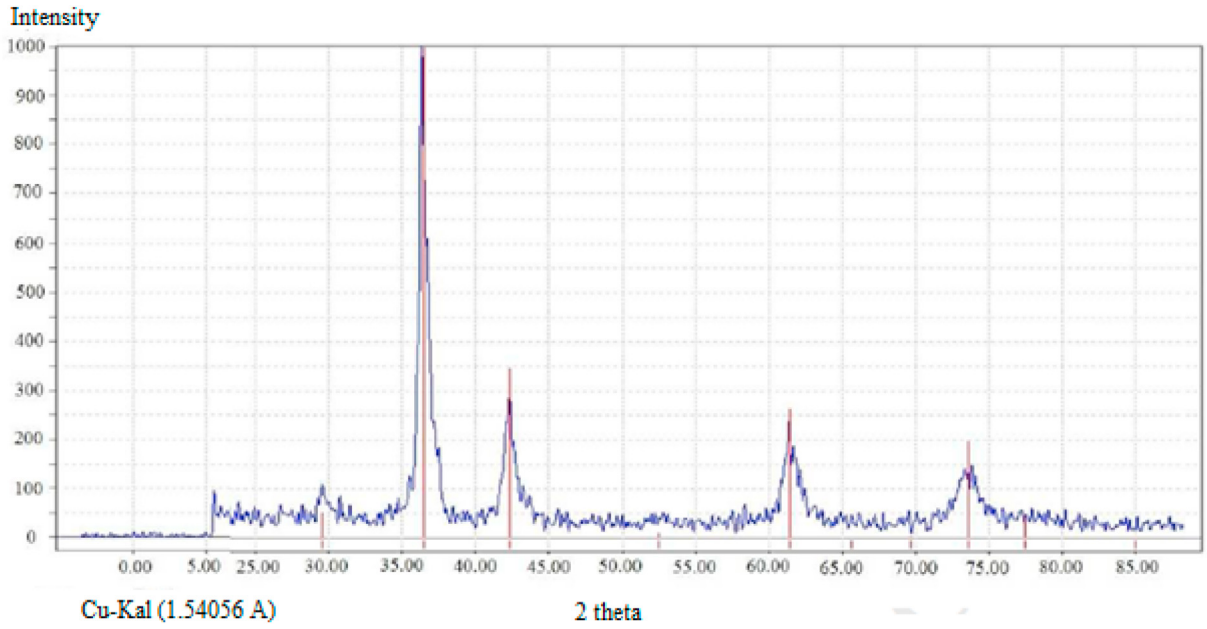

Fig. 2. XRD image of Cu−O nanoparticles.

averaging the three temperatures indicated by the three thermocouples inside the tank. In addition, the temperature of the working fluid inside the evacuated tube was regarded as the average of four shown temperatures inside the tube. The thermocouples were positioned in the central part of the evacuated tube. Similar to the commercial ETSCs, the tube length of the METSC is 180 cm with identical physical properties regarding the absorption surface. Furthermore, the apparatus of the METSC has been shown next to a commercial ETSC in Fig. 6 (b) for denoting the structural modification.

4. Methodology

4.1. Thermodynamic investigation of the METSC

The daily thermal efficiency of the solar collector can be acquired by Eq. (1) (Sadeghi et al., 2019a).

$$\eta = \frac{m_T C_p \Delta T}{A_c G \times t} \tag{1}$$

The related nanofluid-based formula for calculation of C_p can be obtained from (Sadeghi et al., 2019a):

$$C_{p,nf} = \frac{\left[\phi \rho_{np} C_{p,np} + (1-\phi)\rho_{bf} C_{p,bf}\right]}{\rho_{nf}} \tag{2}$$

where ρ_{nf} is the density of the nanofluid defined as:

$$\rho_{nf} = \phi \rho_{np} + (1-\phi)\rho_{bf} \tag{3}$$

Moreover, the energy efficiency of the solar collectors can also be written as follows (Duffie and Beckman, 2013):

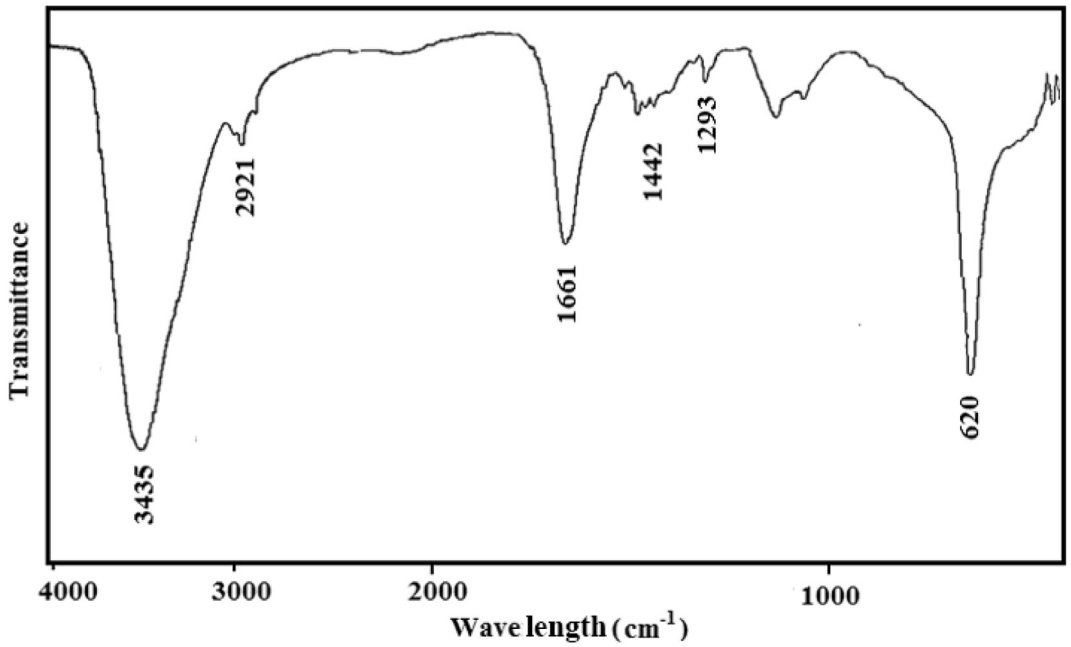

Fig. 3. FT-IR analysis of the proposed nanofluid.

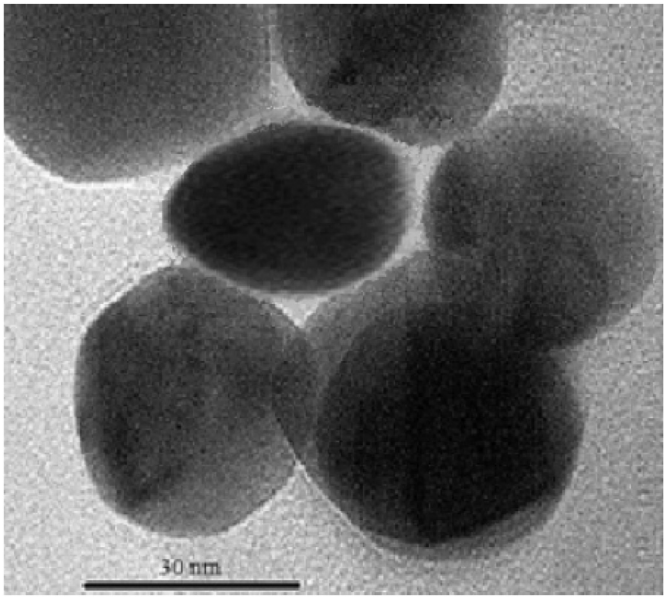

Fig. 4. Transmission Electron Microscope (TEM) view of Cu–O nanoparticles.

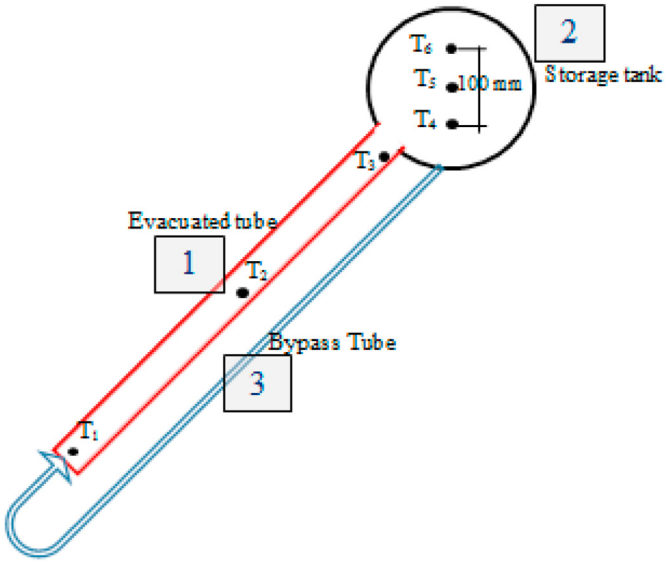

Fig. 5. Schematic of the constructed METSC.

$$\eta = F_R(\tau\alpha)_{ef} - F_R U_L\left(\frac{T_{f,i} - T_a}{G}\right) \quad (4)$$

where F_R is the removal factor, $(\tau\alpha)_{ef}$ is the collector effective transmittance-absorptance multiplication, U_L is the heat loss coefficient, G, is the solar radiation intensity on tubes and ΔT is the fluid temperature difference every 1 h from 9:00 a.m. to 6 p.m., which was the period of time, at which the experiment was carried out. Moreover, $\left(\frac{T_{f,i}-T_a}{G}\right)$ is called reduced temperature, against which the energy efficiency is plotted.

4.2. Methodology for data analysis

ANNs have widely been used as efficient tools to recognize the characteristics and performance parameters of complex and multi-factorial systems such as METSCs. There are some reassuring types of ANN techniques, which are applicative in engineering problems, such as MLP and RBF. In the following, brief explanations of each type are presented.

4.2.1. MLP network

The ANN type selecting depends on the properties of the existence challenge, which must be cleared. For instance, in prediction issues, MLP is one of the most popular networks (Voyant et al., 2017). Actually, MLP network is a feed forward sort of ANNs

Table 1
Properties of the constructed METSC.

Specification	Unit	Dimension and materials
Area of absorber	m^2	0.212
Modified tube length	m	1.5
Rigid body length	m	0.3
Length of the evacuated tube	m	1.8
Bypass pipe length	m	2.1
Width of collector	m	1.2
Number of evacuated tubes	–	1
Diameters of the examined bypass tubes	mm	6,7,8,9,10
Volumes of the examined storage tanks	l	5,6,7,8
Temperature range	K	285–371
Tilt angle of collector	Degree (°)	45
Material of the tank	–	Polyethylene
Sensor of temperature	K-type	15
Absorptivity	–	0.96
Emissivity	–	0.06
Collector transmittance	–	0.91
Outer diameter of tube	m	0.058
Inner diameter of tube	m	0.048
Substance of glass	–	Borosilicate
Substance of sealing method	–	Silicone
Substance of frame	–	Galvanized iron
Substance of insulation	–	Polyethylene
Substance of bypass pipe	–	Polyethylene

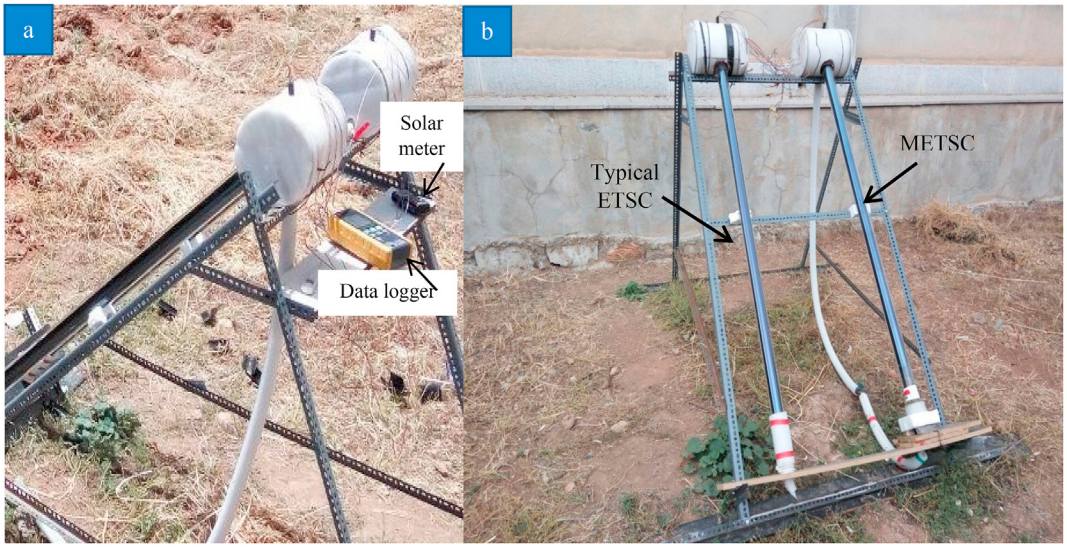

Fig. 6. (a) View of the experimental setup, (b) The apparatus of the METSC water heater.

containing at least one hidden layer. Each layer contains many neurons. Each neuron activates using a function by summing the weights and output from the previous layer plus a fixed bias (Johns and Burkes, 2017). This function called activation function. The sigmoid functions (logsig) and hyperbolic tangent (tansig) are the most prevalent activation functions in neurons. The ANN designers set the hidden layers number and number of neurons per hidden layers within training procedure to balance the precision (Johns and Burkes, 2017). This trend will be carried out for two data sets as training data set and test data set. The prototype architecture of a MLP network is illustrated in Fig. 7. In this architecture, j is the number of inputs (I) and k is the number of outputs (Y). Therefore, the outputs can be achieved by:

$$Y_k(n) = \sum f_n(y(n-1).W_{in}) + b_{in} \quad (5)$$

In the above equation n, b, Wi and f_n represent the number of hidden layers, the neurons bias terms, the weighting factors and the hidden layers activation function.

In this work, MATLAB R2016a software was used to train the MLP model and Levenberg-Marquardt (LM) algorithm will be applied for training process due to its stable and quick convergence (Shi et al., 2017). LM algorithm not only has a faster convergence than basic method of Newton's optimization algorithm, but also is very simple than Newton's optimization algorithm (Sarabakha et al., 2017).

The structure of the utilized MLP is illustrated in Fig. 8. This

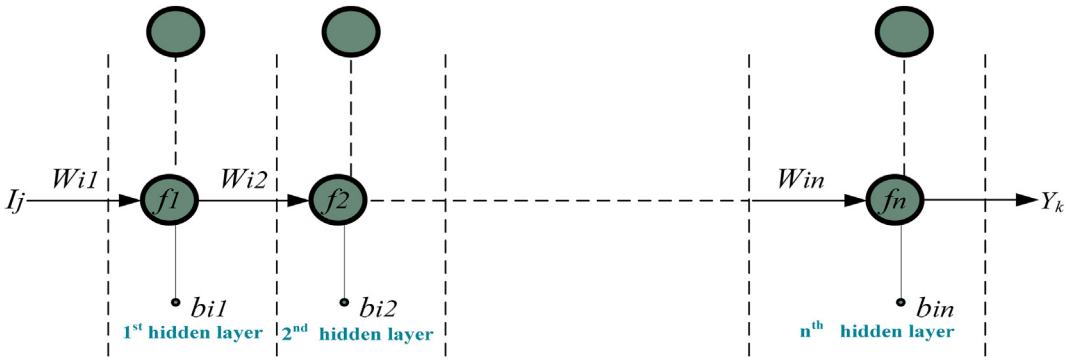

Fig. 7. The prototype architecture of a MLP Network.

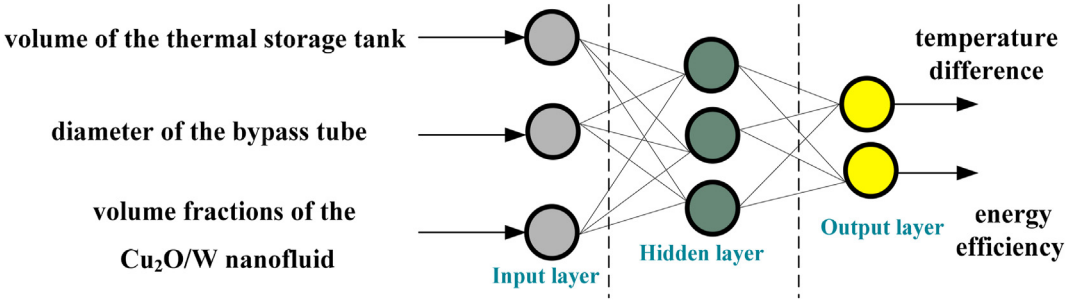

Fig. 8. Model architecture of the designed MLP ANN.

Table 2
The configuration of the MLP model.

No.	MLP Characteristics
Input layer neurons	3
Hidden layer neurons	3
Output layer neurons	2
Selected epochs	3000
Activation function	tansig

structure is comprised of three inputs. They are volume of the thermal storage tank, diameter of the bypass tube, and volumetric concentration of the Cu_2O/DW nanofluid. The output of the architecture contains fluid temperature difference, and the thermal energy efficiency of METSC. The MLP designer should minimize the number of hidden layers and the number of neurons in each layer (Roshani et al., 2017). The designed network is an optimized one with only one hidden layer containing only three neurons. As shown in Table A1 and Table A2, the training and test datasets are obtained from the numerical data: 70% as training data and 30% as test data. The specs of the proposed MLP model are illustrated in Table 2.

4.2.2. RBF network

The RBF is another feedforward type of the ANNs with specified three layers. Its structure is very similar to that of the MLP network that was designed in Fig. 8. It has only one hidden layer at all, generally with a Gaussian activation function for every neuron in this layer. The input layer contains the input features, and the output layer has neurons with linear function for transferring the output features (Rakhshkhorshid, 2017). Miniaturized structure, fast training, appropriate generalization capability, and ability of online learning in comparison with other feedforward ANNs are some benefits of the RBF (Niroomand-Toomaj et al., 2017). The conventional topology of an RBF is illustrated in Fig. 9. The RBF calculates the distance between the input vectors and the weight vectors and carries out it by a Gaussian function. So, the output can be obtained from (Ehsan et al., 2018; Wang et al., 2017):

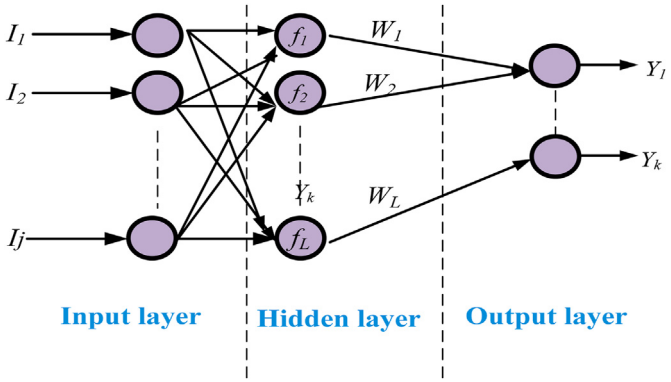

Fig. 9. Conventional Architecture of a RBF network.

Table 3
The configuration of the RBF model.

No.	RBF Characteristics
Input layer neurons	3
Hidden layer neurons	25
Output layer neurons	2
Spread	0.1
Target Error	0
Type of function for activation	Gaussian

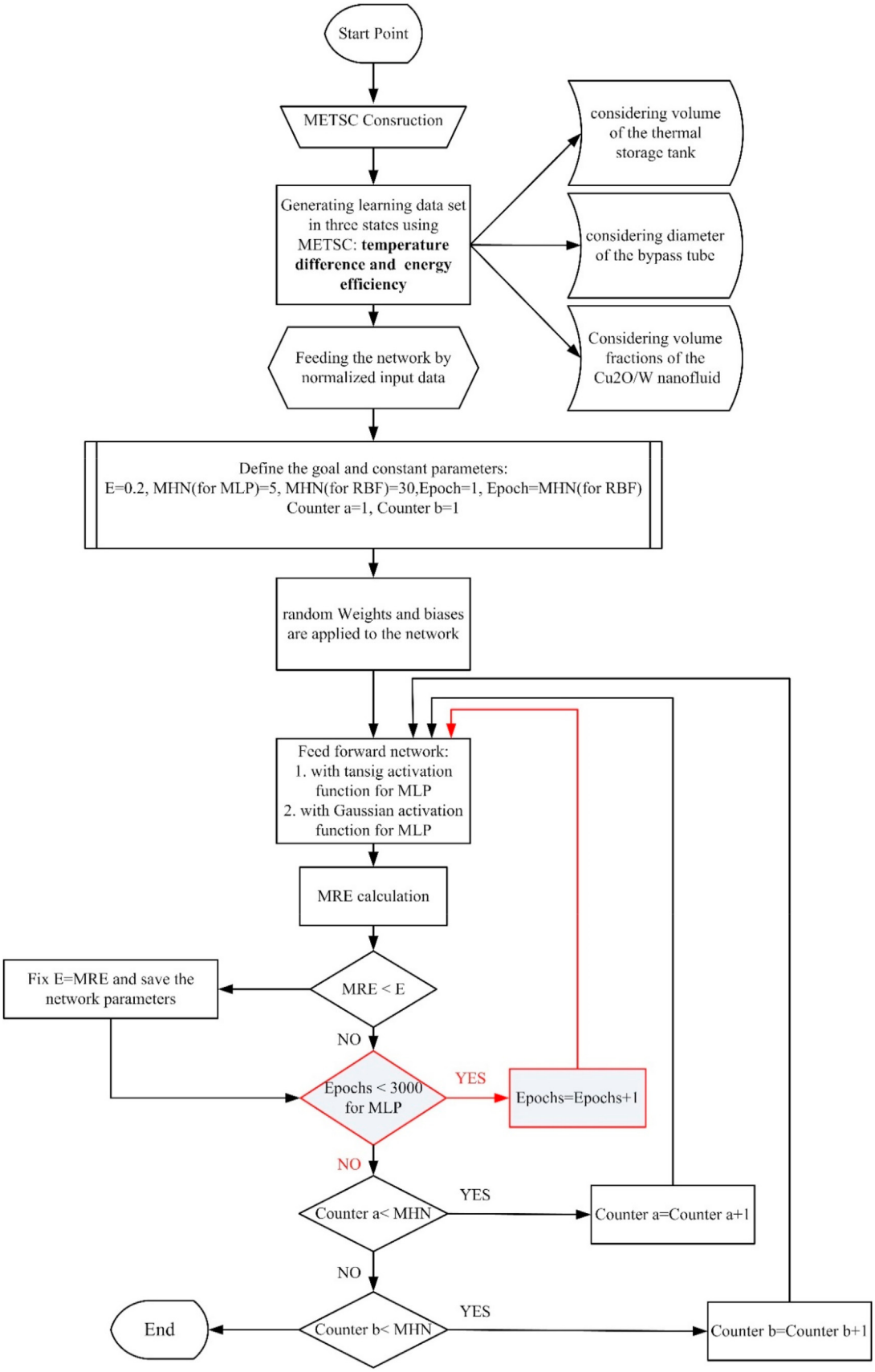

Fig. 10. The study flowchart (regarding the RBF method, the colored part should be eliminated).

Table 4
The highest uncertainties for the METSC operational conditions.

Devices and parameters	MA	Verified range	Uncertainty amount
Thermocouples	0.1 °C	−100-1200 °C	5.7%
Valve	1 m^3/h	0–100 m^3/h	57.8%
Anemometer	0.1 m/s	0.1–35 m/s	5.7%
Pyranometer	0.1 W/m^2	0–2000 W/m^2	5.7%
Thermal performance	–	–	3.3%

$$Y_k = \sum_{j=1}^{L} W_j f_j = \sum_{j=1}^{L} W_j \exp\left(-\frac{1}{2\sigma^2} I - C_j^2 \right) \quad (6)$$

where C_j is determined through the K-means clustering procedure.

As the same as MLP model, the volume of the thermal storage tank, the bypass pipe diameter, volumetric fractions of the Cu_2O/DW nanofluid, fluid temperature difference, and the thermal energy efficiency of the METSC (as detailed in Tables A.1 and A.2) are performed as input and output layers. So, the architecture of the proposed RBF model is very similar to Fig. 7, and the only difference is in the number of the neurons in the hidden layer. The specs of the RBF model are illustrated in Table 3. Fig. 10 represents the flowchart of the implemented AI-based study, in order to give a broader insight.

4.3. Error analysis and uncertainty analysis

These errors include mean relative error percentage (MRPE), mean absolute error percentage (MAPE), and root mean square error (RMSE) having been defined as (Hayati et al., 2014; Roshani et al., 2014; Sadighzadeh et al., 2014):

$$MRPE = 100 \times \frac{1}{N} \sum_{i=1}^{N} \left| \frac{X_i(Ex) - X_i(Pr)}{X_i(Ex)} \right| \quad (7)$$

$$RMSE = 100 \times \left[\frac{\sum_{i=1}^{N} (X_i(Ex) - X_i(Pr))^2}{N} \right] \quad (8)$$

$$MAPE = \frac{1}{N} \sum_{i=1}^{Z} |X_i(Ex) - X_i(Pr)| \quad (9)$$

in which N, '$X\,(Ex)$' and '$X\,(Pr)$' are the number of data, the value of experimental data and the value of the predicted data by MLP, respectively.

Experimental researches are reliable if there does not exist a considerable difference between the results with a slight deviation from the measured amounts of parameters. For the most part, the acquired errors emanate from acquisition of data, reducing data, unreliability of the devices, various environmental and experimental circumstances, etc. In the current work, the standard amount of uncertainty for each device has been calculated from (Kirkup and Frenkel, 2006):

$$u = \frac{MA}{\sqrt{3}} \quad (10)$$

furthermore, the error measurement for the thermal performance of the METSC has been undertaken according to Eq. (11) (Sadeghi et al., 2019b):

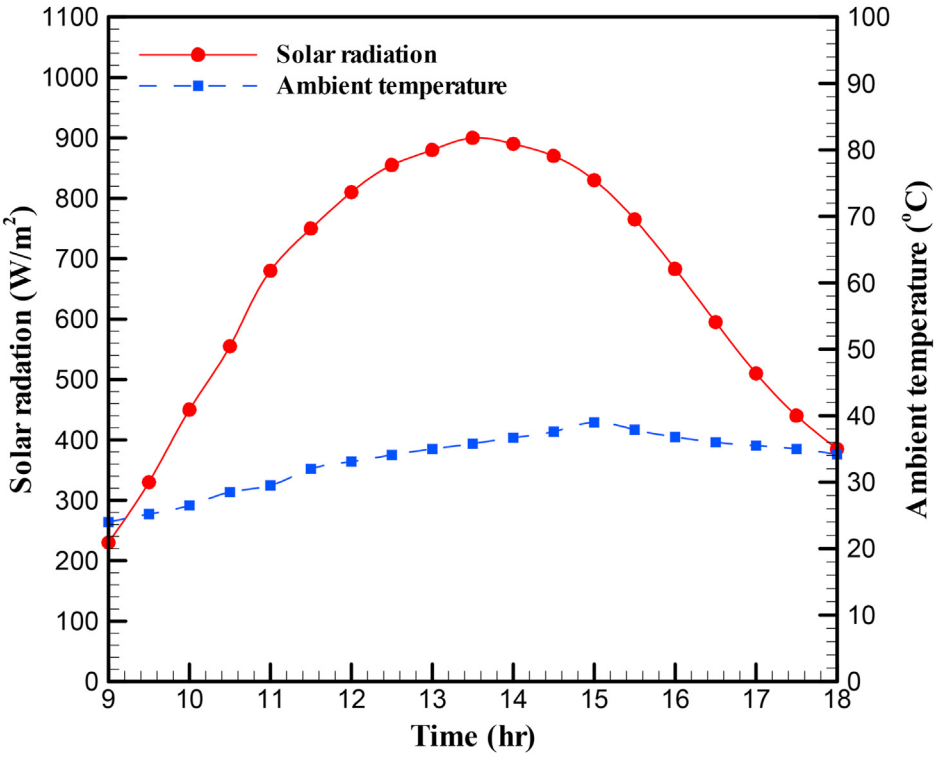

Fig. 11. Average solar radiation and ambient temperature during the time of experiments.

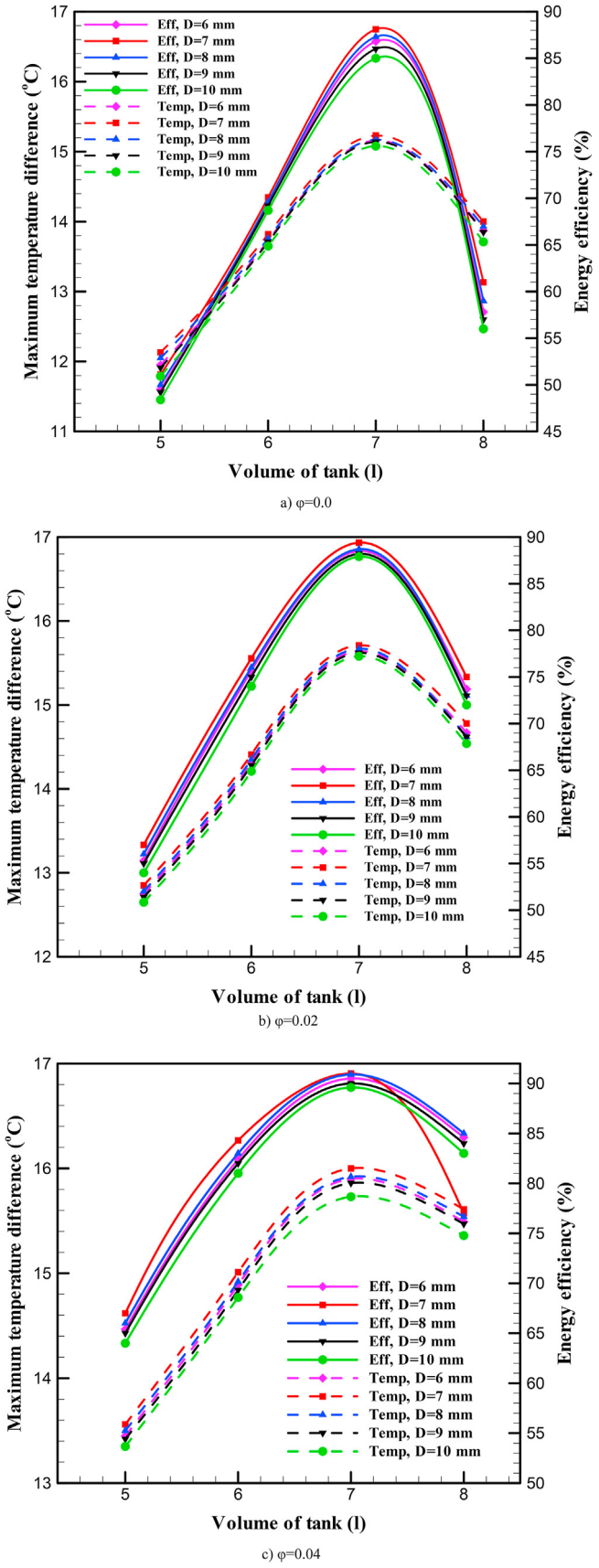

Fig. 12. Maximum hourly fluid temperature difference and energy efficiency of the METSC with respect to volume of thermal storage tank considering various diameters of the bypass pipe, (a) for water as the working fluid ($\phi = 0.0$), (b) for 0.02 vol fraction of the Cu_2O/DW nanofluid ($\phi = 0.02$), (c) for 0.04 vol fraction of the Cu_2O/DW nanofluid ($\phi = 0.04$).

$$\Delta\eta = \left[\left(\frac{\partial\eta}{\partial\rho_f}\Delta\rho_f\right)^2 + \left(\frac{\partial\eta}{\partial T_i}\Delta T_i\right)^2 + \left(\frac{\partial\eta}{\partial T_f}\Delta T_f\right)^2 + \left(\frac{\partial\eta}{\partial G}\Delta G\right)^2\right]^{\frac{1}{2}} \quad (11)$$

The highest amounts of uncertainties for the proposed METSC water heater are represented in Table 4.

5. Results

In this part, the values of solar irradiance on the collector surface during implementing the experimentations are indicated hourly. Then, the effects of applying Cu_2O/DW nanofluid on the maximum hourly fluid temperature difference inside the METSC, and its thermal performance are surveyed through experiments. Finally, the energy efficiency and the fluid temperature difference were modelled through MLP and RBF techniques, and the obtained results were compared to one another.

5.1. Results from the experimental investigations

5.1.1. Solar radiation and ambient temperature

The amount of solar radiation throughout the experimentation time and the ambient temperature were measured experimentally. As indicated in Fig. 11, the highest amounts of solar radiation and ambient temperature are roughly 900 (W/m^2) and 39 °C, respectively. Moreover, the highest solar radiation precedes the highest ambient temperature because after receiving the highest solar radiation around the solar noon, the Earth starts to emit an extent of the absorbed heat to the sky and surroundings leading to a rise in the ambient temperature. In other words, the highest ambient temperature was recorded when the highest emission of heat from the Earth to the sky was happening.

5.1.2. Thermal investigations

The daily energy efficiency and the maximum hourly fluid temperature difference are illustrated in Fig. 12 considering different diameters of the bypass pipe. Fig. 12 (a) shows that the highest daily energy efficiency and the maximum hourly fluid temperature difference were recorded for the bypass pipe diameter of 7 mm. In fact, as the bypass pipe diameter enhances the volumetric flow rate and the flow between the storage tank and the evacuated tube also rises; hence, the maximum hourly fluid temperature difference and the energy efficiency of the METSC decrease. On the other hand, the optimum volume of storage tank for the METSC containing one tube within the experimentations was reported as 7 l. If the volume of tank becomes more than 7 l, the heat flow equivalence between the volume of tank and the volume of the evacuated tube becomes disrupted; thereby, the maximum water temperature difference and the energy efficiency of the METSC reduce.

Fig. 12 (b) and (c) similarly represent that the optimized volume of the thermal storage tank is 7 l, and the optimum bypass pipe diameter is 7 mm. They indicate that the similar trends hold for change of fluid temperature difference and maximum energy efficiency of the METSC when nanofluid is applied to the solar system as the working fluid; however, utilizing nanofluid increases these quantities to some extent. Using Cu_2O/DW nanofluid at volume fractions of 0.2 and 0.04 increases the energy efficiency of the METSC up to 1% and 3%, respectively. Moreover, increasing the concentration of the Cu_2O nanoparticles in the base fluid (distilled

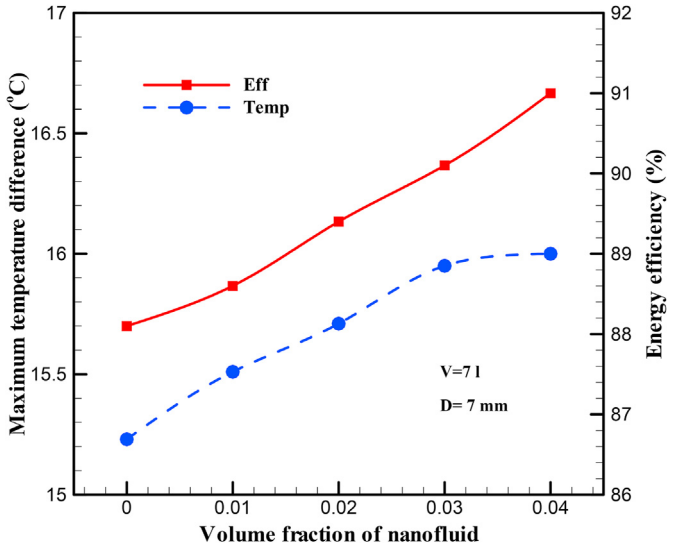

Fig. 13. Influence of changing volumetric fraction of the Cu_2O/DW nanofluid on the maximum hourly fluid temperature difference and maximum energy efficiency of the optimum METSC.

Table 5
The calculated errors for the designed MLP network.

Error	Train (ΔT)	Test (ΔT)	Train (η)	Test (η)
MRPE	0.00564	0.01262	0.00504	0.57616
MAPE	8.98e-04	6.98e-04	0.00403	0.00741
RMSE	0.00108	8.97e-04	0.00531	0.01728

water) leads to better performance of the METSC. It is observed that the maximum fluid temperature difference inside tank and the maximum energetic performance of METSC at 0.04 vol fraction of the nanoparticle are 16 °C and 0.91, respectively. Finally, it can be concluded that changing the volume of tank more tangibly affects the performance of the METSC compared to altering the diameter of the bypass tube or using the proposed nanofluid. At the volume fraction of 0.04 nanoparticles, the amounts of energy efficiencies of the METSC for volumes of the storage tanks of 5, 6, 7, and 8 l were 0.67, 0.84, 0.91, and 0.77, respectively.

5.1.3. On the role of Cu_2O/DW nanofluid

Fig. 13 demonstrates that enhancing the concentration of Cu_2O/DW nanofluid leads to rises in both maximum hourly fluid

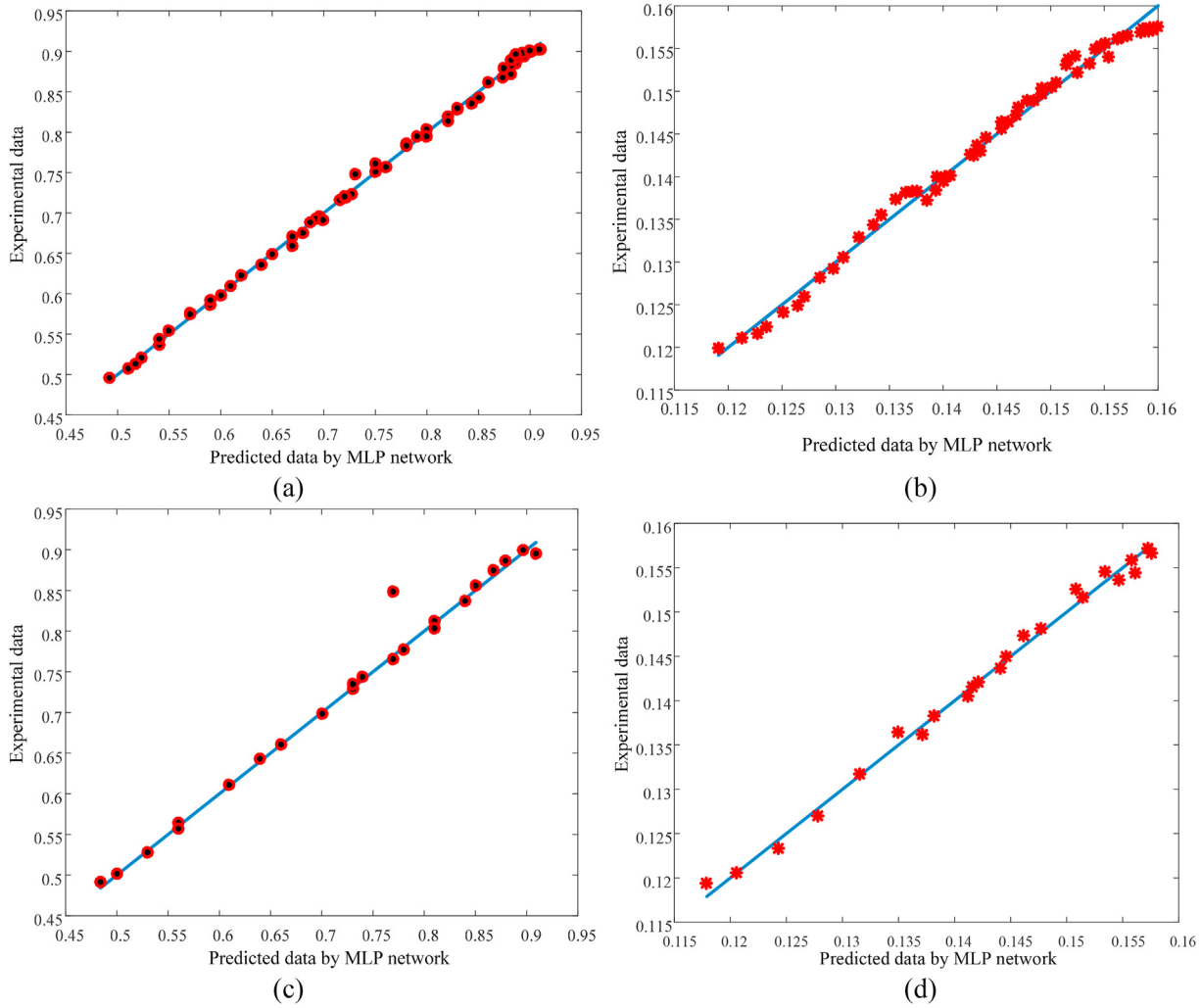

Fig. 14. Train and test regression diagrams for two outputs using MLP model (a) temperature difference training (b) energy efficiency training (c) maximum fluid temperature difference test (d) energy efficiency test.

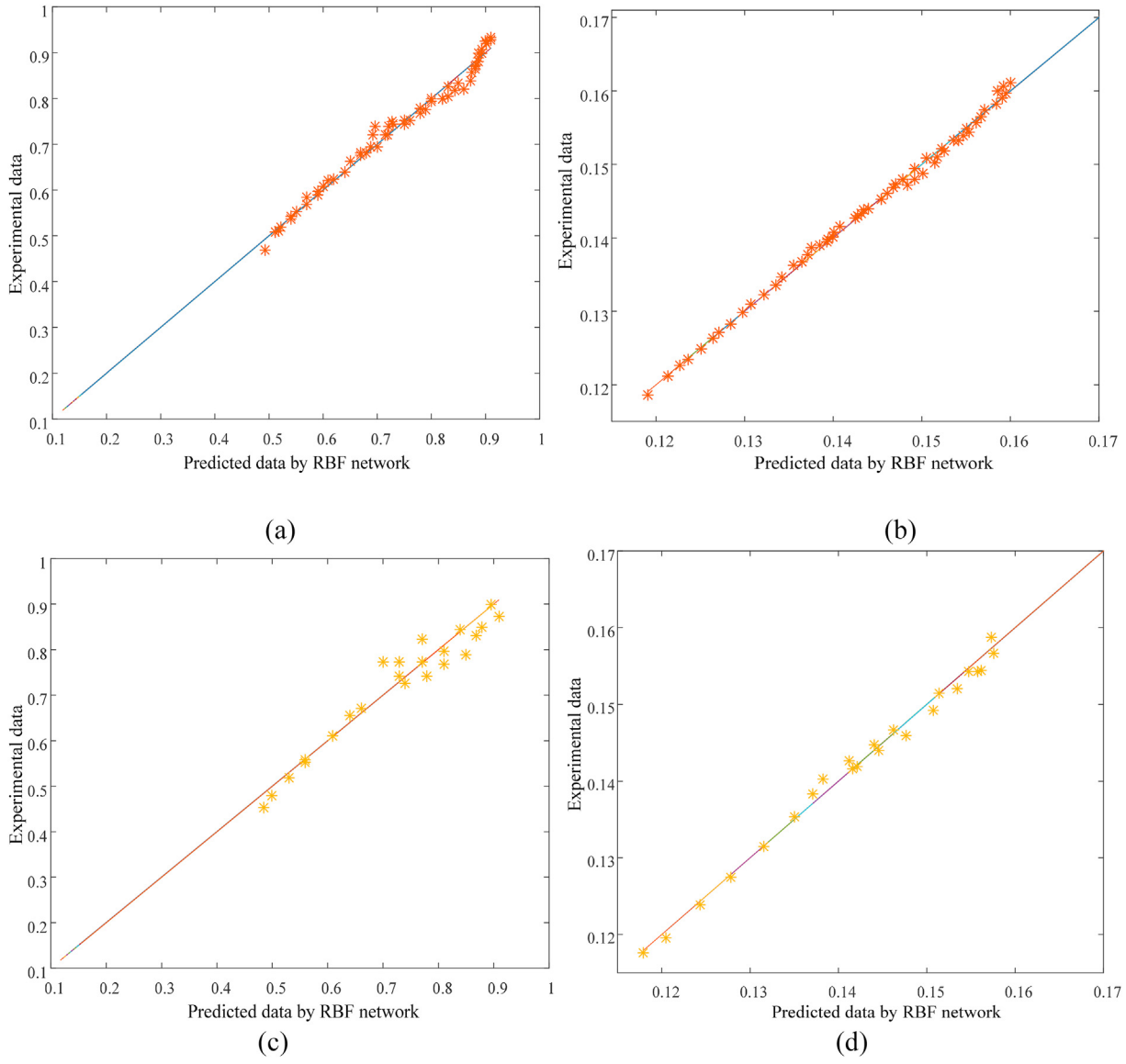

Fig. 15. Train and test regression diagrams for two outputs using RBF model (a) temperature difference training (b) energy efficiency training (c) temperature difference test (d) energy efficiency test.

Table 6
Calculated errors for the designed RBF network.

Error	Train (ΔT)	Test (ΔT)	Train (η)	Test (η)
MRPE	0.00136	0.14901	0.04431	0.90722
MAPE	4.4e-04	8.6e-04	0.01204	0.02408
RMSE	6.0e-04	0.00106	0.01565	0.03117

temperature difference and maximum energy efficiency of the METSC. Adding the nanoparticles to the base fluid leads to more heat absorption; consequently, more solar radiation will be absorbed by the nanofluid. In fact, nanoparticles increase the specific heat of the fluid resulting in enhancing ΔT and η. On the other hand, adding nanoparticles to the base fluid increases the Brownian motion between the particles leading to an increase in the conductivity of the fluid, which causes the METSC to present better thermal performance. Regarding the optimum METSC (volume of tank 7 l and bypass pipe diameter of 7 mm) the energy efficiencies at the volume fractions of 0, 0.01, 0.02, and 0.04 the utilized nanofluid were 0.881, 0.889, 0.89, 0.9, and 0.91, respectively.

5.2. Results from ANN modelling

5.2.1. MLP modelling

The MLP predicted in comparison with the experimental results are depicted for training and test process as shown in Fig. 14. In addition, Table 5 illustrates the calculated errors as to the offered MLP model. As can be concluded from Table 5, there is very low calculated errors for both the training and the test datasets for both outputs, especially for the first output (maximum hourly temperature difference of the fluid).

5.2.2. RBF modelling

The regression diagrams for training and testing process using RBF model are depicted in Fig. 15.

Table 6indicates the gained errors defined for the designed RBF network. As it can be concluded based on this Table, there is low obtained errors, especially for the second output (energy efficiency).

As be concluded, the proposed MLP and RBF networks are ideal

to predict the first output (temperature difference) and second output (energy efficiency), respectively. So, the combination of these ANNs is a good predictor to model the METSCs. By comparing these two models, MLP model can be a better predictor in the case of MRPE value. So, using the proposed MLP model, the hourly temperature difference and the daily energy efficiency can be determined by below formulas:

$$\begin{aligned}\Delta T = {} & 0.0195 \times F\Big(10^3(-6.9976 \times V - 2.319 \times D + 1.423 \times \phi) \\ & + 56.42\Big) + 0.314 \times F\Big(10^3(-0.054 \times V + 0.124 \times D \\ & - 0.069 \times \phi) + 12.898\Big) + 0.269 \times F\Big(10^3(-0.027 \times V \\ & + 0.038 \times D - 0.0249 \times \phi) - 7.944\Big) + 0.117\end{aligned} \tag{12}$$

$$\begin{aligned}\eta = {} & 0.222 \times F\Big(10^3(-6.9976 \times V - 2.319 \times D + 1.423 \times \phi) \\ & + 56.42\Big) + 0.048 \times F\Big(10^3(-0.054 \times V + 0.124 \times D \\ & - 0.069 \times \phi) + 12.898\Big) + 0.449 \times F\Big(10^3(0.027 \times V \\ & - 0.038 \times D + 0.0249 \times \phi) - 7.944\Big) + 0.365\end{aligned} \tag{13}$$

where:

$$F(I) = \frac{2}{1 + e^{-2I}} - 1 \tag{14}$$

6. Conclusions

In this study, the experimental investigation of METSC using the Cu_2O/DW nanofluid has been conducted. Moreover, MLP and RBF techniques were exploited to mathematically model the hourly fluid temperature difference and the energy efficiency of the METSCs. An ETSC was structurally modified through a bypass pipe linking the tank to the tube so as to eliminate the stagnant area and make more proportion of the fluid inside the METSC contribute to the heat transfer process. The results demonstrated that in similar conditions, enhancing the volumetric fraction of the Cu_2O/DW nanofluid brings about a rise in thermal characteristics of the METSC. On the basis of the experimental observations, the optimum characteristics of the single tube METSC regarding the bypass pipe diameter and the volume of tank were reported as 7 mm and 7 l, respectively. It was also concluded that changing the volume of tank influences the thermal performance of METSCs more than alteration of the bypass pipe diameter and the volume fraction of the used nanofluid. Furthermore, the highest energy efficiency and the maximum hourly fluid temperature difference were reported as 0.91 and 16.2 °C for the METSC containing a 7 l volume of tank and 7 mm diameter of bypass pipe at 0.04 vol fraction of the proposed nanofluid. In terms of the ANN techniques, it found that both MLP and RBF techniques are capable of modelling the temperature difference and the energy efficiency of the METSC. However, it was deduced that the MLP technique is more successful in predicting the thermal performance of METSCs by presenting less errors. Regarding the mathematical model for the energy efficiency, the amounts of MRPE, MAPE, and RMSE for the training stage of MLP technique are 0.005, 0.004, and 0.005, successively; whereas, these errors for that of the RBF technique are 0.044, 0.012, and 0.015, respectively.

Even though ANN techniques present reliable models for the performance parameters of the METSCs, other AI techniques, such as GEP, MARS, MT, GA, etc. would be put into practice in order to make a comparison among these techniques for more trustable designing procedure. In addition, in the present work, a closed system was investigated, and it must be experimented whether an increase in the bypass pipe diameter exacerbates the performance of METSCs or not. On the other hand, integrating the METSCs with other solar systems, such as the solar stills and membrane distillation systems might be a reassuring approach and is worth being experimented in the future studies.

CRediT authorship contribution statement

Gholamabbas Sadeghi: Conceptualization, Methodology, implementing the experiments, Writing – original draft, revising the manuscript, I declare that all the authors had a significant scientific contribution to the paper, and all the contents of this paper have been shared with all authors. The roles of all authors are listed as follows. **Anna Laura Pisello:** Supervision, Supervision including mentorship to the core team, editing the manuscript, Validation, contribution to the revision procedures. **Saeed Nazari:** Validation of the experimental results, editing, revision, graphical contents. **Mohammad Jowzi:** Methodology, contribution to the setup construction, data interpretation. **Farzin Shama:** Validation, Conducting the software, writing, validating the numerical results.

Declaration of competing interest

The authors declare that they have no known competing financial interests or personal relationships that could have appeared to influence the work reported in this paper.

References

Abdollahi-Moghaddam, M., Motahari, K., Rezaei, A., 2018. Performance characteristics of low concentrations of CuO/water nanofluids flowing through horizontal tube for energy efficiency purposes; an experimental study and ANN modeling. J. Mol. Liq. 271, 342–352. https://doi.org/10.1016/j.molliq.2018.08.149.

Cabeza, L.F., de Gracia, A., Pisello, A.L., 2018. Integration of renewable technologies in historical and heritage buildings: a review. Energy Build. 177, 96–111. https://doi.org/10.1016/j.enbuild.2018.07.058.

Duffie, J.A., Beckman, W.A., 2013. Solar Engineering of Thermal Processes. John Wiley & Sons.

Ehsan, N., Farzin, S., Salar, M., 2018. Designing a simple radiometric system to predict void fraction percentage independent of flow pattern using radial basis function. Metrol. Meas. Syst. 25, 347—358. https://doi.org/10.24425/119560.

Eidan, A.A., AlSahlani, A., Ahmed, A.Q., Al-fahham, M., Jalil, J.M., 2018. Improving the performance of heat pipe-evacuated tube solar collector experimentally by using Al2O3 and CuO/acetone nanofluids. Sol. Energy 173, 780–788. https://doi.org/10.1016/j.solener.2018.08.013.

Ghafurian, M.M., Dastjerd, F., Afsharian, A., Esfahani, F.R., Niazmand, H., Behzadnia, H., Wongwises, S., Mahian, O., 2020. Low-cost zinc-oxide nanoparticles for solar-powered steam production: superficial and volumetric approaches. J. Clean. Prod. 280, 124261. https://doi.org/10.1016/j.jclepro.2020.124261.

Ghritlahre, H.K., Prasad, R.K., 2018a. Exergetic performance prediction of solar air heater using MLP, GRNN and RBF models of artificial neural network technique. J. Environ. Manag. 223, 566–575. https://doi.org/10.1016/j.jenvman.2018.06.033.

Ghritlahre, H.K., Prasad, R.K., 2018b. Application of ANN technique to predict the performance of solar collector systems-A review. Renew. Sustain. Energy Rev. 84, 75–88. https://doi.org/10.1016/j.rser.2018.01.001.

Ghritlahre, H.K., Prasad, R.K., 2018c. Investigation of thermal performance of unidirectional flow porous bed solar air heater using MLP, GRNN, and RBF models of ANN technique. Therm. Sci. Eng. Prog. 6, 226–235. https://doi.org/10.1016/j.tsep.2018.04.006.

Hamburg, A., Kuusk, K., Mikola, A., Kalamees, T., 2020. Realisation of energy performance targets of an old apartment building renovated to nZEB. Energy 194, 116874. https://doi.org/10.1016/j.energy.2019.116874.

Hayati, M., Shama, F., Roshani, S., Abdipour, A., 2014. Linearization design method in class-F power amplifier using artificial neural network. J. Comput. Electron. 13 (4), 943–949 doi.10.1007/s10825-014-0612-x.

Heng, S.Y., Asako, Y., Suwa, T., Nagasaka, K., 2019. Transient thermal prediction methodology for parabolic trough solar collector tube using artificial neural network. Renew. Energy 131, 168–179. https://doi.org/10.1016/j.renene.2018.07.037.

Iranmanesh, S., Ong, H.C., Ang, B.C., Sadeghinezhad, E., Esmaeilzadeh, A., Mehrali, M., 2017. Thermal performance enhancement of an evacuated tube solar collector using graphene nanoplatelets nanofluid. J. Clean. Prod. 162, 121–129. https://doi.org/10.1016/j.jclepro.2017.05.175.

Johns, J.M., Burkes, D., 2017. Development of multilayer perceptron networks for isothermal time temperature transformation prediction of U-Mo-X alloys. J. Nucl. Mater. 490, 155–166. https://doi.org/10.1016/j.jnucmat.2017.03.050.

Johnsson, J., Adl-Zarrabi, B., 2020. A numerical and experimental study of a pavement solar collector for the northern hemisphere. Appl. Energy 260, 114286. https://doi.org/10.1016/j.apenergy.2019.114286.

Jowzi, M., Veysi, F., Sadeghi, G., 2019. Experimental and numerical investigations on the thermal performance of a modified evacuated tube solar collector: effect of the bypass tube. Sol. Energy 183, 725–737. https://doi.org/10.1016/j.solener.2019.03.063.

Kabeel, A., Abdelgaied, M., Elrefay, M.K., 2020. Thermal performance improvement of the modified evacuated U-tube solar collector using hybrid storage materials and low-cost concentrators. J. Energy Storage 29, 101394. https://doi.org/10.1016/j.est.2020.101394.

Khan, M., Ullah, M., Iqbal, T., Mahmood, H., Khan, A.A., Shafique, M., Majid, A., Ahmed, A., Khan, N.A., 2015. Surfactant assisted synthesis of cuprous oxide (Cu2O) nanoparticles via solvothermal process. Nano Sci. Nano Tech. Res. 3 (1), 16–22 doi.10.12691/nnr-3-1-3.

Kirkup, L., Frenkel, R.B., 2006. An Introduction to Uncertainty in Measurement: Using the GUM (Guide to the Expression of Uncertainty in Measurement). Cambridge University Press.

Lidberg, T., Olofsson, T., Ödlund, L., 2019. Impact of domestic hot water systems on district heating temperatures. Energies 12 (24), 4694. https://doi.org/10.3390/en12244694.

López-Ochoa, L.M., Verichev, K., Las-Heras-Casas, J., Carpio, M., 2019. Solar domestic hot water regulation in the Latin American residential sector with the implementation of the energy performance of buildings directive: the case of Chile. Energy 188, 115985. https://doi.org/10.1016/j.energy.2019.115985.

Ma, T., Li, M., Kazemian, A., 2020. Photovoltaic thermal module and solar thermal collector connected in series to produce electricity and high-grade heat simultaneously. Appl. Energy 261, 114380. https://doi.org/10.1016/j.apenergy.2019.114380.

Morrison, G., Budihardjo, I., Behnia, M., 2004. Water-in-glass evacuated tube solar water heaters. Sol. Energy 76 (1–3), 135–140. https://10.1016/j.solener.2003.07.024.

Nazari, S., Safarzadeh, H., Bahiraei, M., 2019a. Experimental and analytical investigations of productivity, energy and exergy efficiency of a single slope solar still enhanced with thermoelectric channel and nanofluid. Renew. Energy 135, 729–744. https://doi.org/10.1016/j.renene.2018.12.059.

Nazari, S., Safarzadeh, H., Bahiraei, M., 2019b. Performance improvement of a single slope solar still by employing thermoelectric cooling channel and copper oxide nanofluid: an experimental study. J. Clean. Prod. 208, 1041–1052. https://doi.org/10.1016/j.jclepro.2018.10.194.

Nazari, S., Bahiraei, M., Moayedi, H., Safarzadeh, H., 2020. A proper model to predict energy efficiency, exergy efficiency, and water productivity of a solar still via optimized neural network. J. Clean. Prod. 277, 123232. https://doi.org/10.1016/j.jclepro.2020.123232.

Niroomand-Toomaj, E., Etemadi, A., Shokrollahi, A., 2017. Radial basis function modeling approach to prognosticate the interfacial tension CO2/Aquifer Brine. J. Mol. Liq. 238, 540–544. https://doi.org/10.1016/j.molliq.2017.04.135.

Olfian, H., Ajarostaghi, S.S.M., Ebrahimnataj, M., 2020. Development on evacuated tube solar collectors: a review of the last decade results of using nanofluids. Sol. Energy 211, 265–282. https://doi.org/10.1016/j.solener.2020.09.056.

Pigliautile, I., Castaldo, V.L., Makaremi, N., Pisello, A.L., Cabeza, L.F., Cotana, F., 2019. On an innovative approach for microclimate enhancement and retrofit of historic buildings and artworks preservation by means of innovative thin envelope materials. J. Cult. Herit. 36, 222–231. https://doi.org/10.1016/j.culher.2018.04.017.

Qiu, L., Zhu, N., Feng, Y., Michaelides, E.E., Żyła, G., Jing, D., Zhang, X., Norris, P.M., Markides, C.N., Mahian, O., 2020. A review of recent advances in thermophysical properties at the nanoscale: from solid state to colloids. Phys. Rep. 843, 1–81. https://doi.org/10.1016/j.physrep.2019.12.001.

Rakhshkhorshid, M., 2017. A robust RBF-ANN model to predict the hot deformation flow curves of API X65 pipeline steel. Iran. J. Mater. Form. 4 (1), 12–20. https://doi.org/10.22099/ijmf.2017.3941.

Roshani, G., Eftekhari-Zadeh, E., Shama, F., Salehizadeh, A., Methods, 2017. Combined application of neutron activation analysis using IECF device and neural network for prediction of cement elements. Radiat. Detect Technol Methods 1 (2), 23. https://doi.org/10.1007/s41605-017-0025-z.

Roshani, G.H., Feghhi, S.A.H., Shama, F., Salehizadeh, A., Nazemi, E., 2014. Prediction of materials density according to number of scattered gamma photons using optimum artificial neural network. J. Comput. Methods Phys. 305345. https://doi.org/10.1155/2014/305345, 2014.

Rosso, F., Pisello, A.L., Cotana, F., Ferrero, M., 2014. Integrated thermal-energy analysis of innovative translucent white marble for building envelope application. Sustainability 6 (8), 5439–5462. https://doi.org/10.3390/su6085439.

Sabiha, M., Saidur, R., Mekhilef, S., Mahian, O., 2015. Progress and latest developments of evacuated tube solar collectors. Renew. Sustain. Energy Rev. 51, 1038–1054. https://doi.org/10.1016/j.rser.2015.07.016.

Sadeghi, G., Najafzadeh, M., Ameri, M., 2020a. Thermal characteristics of evacuated tube solar collectors with coil inside: an experimental study and evolutionary algorithms. Renew. Energy 151, 575–588. https://doi.org/10.1016/j.renene.2019.11.050.

Sadeghi, G., Najafzadeh, M., Safarzadeh, H., 2020b. Utilizing gene-expression programming in modelling the thermal performance of evacuated tube solar collectors. J. Energy Storage 30, 101546. https://doi.org/10.1016/j.est.2020.101546.

Sadeghi, G., Nazari, S., 2021. Retrofitting a thermoelectric-based solar still integrated with an evacuated tube collector utilizing an antibacterial-magnetic hybrid nanofluid. Desalination 500, 114871. https://doi.org/10.1016/j.desal.2020.114871.

Sadeghi, G., Nazari, S., Ameri, M., Shama, F., 2020c. Energy and exergy evaluation of the evacuated tube solar collector using Cu2O/water nanofluid utilizing ANN methods. Sustain. Energy Technol. Assess. 37, 100578. https://doi.org/10.1016/j.seta.2019.100578.

Sadeghi, G., Pisello, A.L., Safarzadeh, H., Poorhossein, M., Jowzi, M., 2020d. On the effect of storage tank type on the performance of evacuated tube solar collectors: solar radiation prediction analysis and case study. Energy 117331. https://doi.org/10.1016/j.energy.2020.117331.

Sadeghi, G., Safarzadeh, H., Ameri, M., 2019a. Experimental and numerical investigations on performance of evacuated tube solar collectors with parabolic concentrator, applying synthesized Cu2O/distilled water nanofluid. Energy Sustain Dev 48, 88–106. https://doi.org/10.1016/j.esd.2018.10.008.

Sadeghi, G., Safarzadeh, H., Bahiraei, M., Ameri, M., Raziani, M., 2019b. Comparative study of air and argon gases between cover and absorber coil in a cylindrical solar water heater: an experimental study. Renew. Energy 135, 426–436. https://doi.org/10.1016/j.renene.2018.12.030.

Sadighzadeh, A., Salehizadeh, A., Mohammadzadeh, M., Shama, F., Setayeshi, S., Feghhi, S., Sadati, S., Rezaei, M., Haji Ebrahimi, E., Roshani, G.H., 2014. Prediction of neutron yield of IR-IECF facility in high voltages using artificial neural network. J. Eng. 798160. https://doi.org/10.1155/2014/798160, 2014.

Sanjeevi, B., Loganathan, K., 2020. Synthesis OF multi wall carbon nanotubes nanofluid BY using two step method. Therm. Sci. 24, 519–524. https://doi.org/10.2298/TSCI190414430S.

Sarabakha, A., Imanberdiyev, N., Kayacan, E., Khanesar, M.A., Hagras, H., 2017. Novel Levenberg–Marquardt based learning algorithm for unmanned aerial vehicles. Inf. Sci. 417, 361–380. https://doi.org/10.1016/j.ins.2017.07.020.

Sato, A.I., Scalon, V.L., Padilha, A., 2012. Numerical analysis of a modified evacuated tubes solar collector. International Conference on Renewable Energies and Power Quality (ICREPQ'12) Santiago de Compostela (Spain), 28th to 30th March. https://doi.org/10.24084/repqj10.322.

Shah, M.A., Al-Ghamdi, M., 2011. Preparation of copper (Cu) and copper oxide (Cu2O) nanoparticles under supercritical conditions. Mater. Sci. Appl. 2 (8), 977–980 doi.10.4236/msa.2011.28131.

Sharafeldin, M., Grof, G., 2018. Evacuated tube solar collector performance using CeO2/water nanofluid. J. Clean. Prod. 185, 347–356. https://doi.org/10.1016/j.jclepro.2018.03.054.

Sheikholeslami, M., Mahian, O., 2019. Enhancement of PCM solidification using inorganic nanoparticles and an external magnetic field with application in energy storage systems. J. Clean. Prod. 215, 963–977. https://doi.org/10.1016/j.jclepro.2019.01.122.

Shi, X., Feng, Y., Zeng, J., Chen, K., 2017. Chaos time-series prediction based on an improved recursive Levenberg–Marquardt algorithm. Chaos, Solit. Fractals 100, 57–61. https://doi.org/10.1016/j.chaos.2017.04.032.

Voyant, C., Notton, G., Darras, C., Fouilloy, A., Motte, F., 2017. Uncertainties in global radiation time series forecasting using machine learning: the multilayer perceptron case. Energy 125, 248–257. https://doi.org/10.1016/j.energy.2017.02.098.

Wang, L., Liu, J., Yan, Y., Wang, X., Wang, T., 2017. Gas-liquid two-phase flow measurement using coriolis flowmeters incorporating artificial neural network, support vector machine, and genetic programming algorithms. IEEE Trans Instrum Meas 66 (5), 852–868. https://doi.org/10.1109/TIM.2016.2634630.

Zhao, J., Pan, R., Sun, R., Wen, C., Zhang, S.-L., Wu, B., Nyholm, L., Zhang, Z.-B., 2019. High-conductivity reduced-graphene-oxide/copper aerogel for energy storage. Nanomater. Energy 60, 760–767. https://doi.org/10.1016/j.nanoen.2019.04.023.